Dissymmetrical *trans*-Ethynyl-Butadiynyl Adducts on a Diruthenium Core: Synthesis, Characterization, and Selective Deprotection

Tong Ren*

Department of Chemistry and Center for Supramolecular Science, University of Miami, Coral Gables, Florida 33124

Received October 15, 2001

Reactions between the ethynyl complexes (4,0)-$[Ru_2(ap)_4](C_2SiR_3)$ (*ap* is 2-anilinopyridinate, R = ^{i}Pr (**1a**) and CH_3 (**1b**)) and LiC_4SiMe_3 result in the formation of dissymmetrical ethynyl-butadiynyl adducts *trans*-(4,0)-$(Me_3SiC_4)[Ru_2(ap)_4](C_2SiR_3)$ (R = ^{i}Pr (**2a**) and CH_3 (**2b**)). Treating **2b** with K_2CO_3 in MeOH/THF leads to *trans*-$(HC_4)[Ru_2(ap)_4](C_2SiMe_3)$ (**3b**) and *trans*-$(HC_4)[Ru_2(ap)_4](C_2H)$ (**4**) in 86% and ca. 10% yields, respectively, and the former can be quantitatively converted to **4** using NaOH. Treating **2a** with NaOH in MeOH/THF yields *trans*-$(HC_4)[Ru_2(ap)_4](C_2Si^iPr_3)$ (**3a**) only. Single-crystal structural analysis of **2a** and **3b** revealed that the Ru−Ru unit and the axial alkynyl ligands are approximately collinear in both molecules. Rich redox chemistry was revealed for all the compounds through voltammetric study: compound **1** exhibits reversible one-electron oxidation and reduction, and compounds **2**−**4** exhibit one one-electron oxidation and two one-electron reductions. All the ethynyl-butadiynyl adducts (**2**−**4**) exhibit an intense charge-transfer absorption of λ_{max} around 1035 nm, revealing a HOMO−LUMO gap of 1.20 eV.

Introduction

Synthesis of monodisperse conjugated oligomers has attracted much attention recently due to the ubiquitous role of monodisperse conjugated oligomers in both electronic and optoelectronic applications.[1] Among synthetic strategies explored, the divergent−convergent approach has been elegantly demonstrated in the synthesis of hydrocarbon oligomers,[2] where an *orthogonal* synthon is the key. Based on the orthogonal synthon *p*-diethylazaphenylacetylene, monodisperse oligo(*p*-phenylene ethynylene) up to 16mer have been prepared by Tour et al.[3,4] Using *m*-dialkylazaphenylacetylene and related building blocks, Moore and co-workers have realized shape-persistent phenylene ethynylene dendrimers, which further self-assemble into well-defined nano-architectures.[5]

Recently, we succeeded in synthesizing a simple rigid rod (**A** in Scheme 1) by capping the polyyne-diyl chain (C_2 and C_4) with $[Ru_2(ap)_4]$ termini (*ap* = 2-anilinopyridinate) and demonstrated the existence of a significant electronic delocalization between two Ru_2-termini mediated by the polyyne-diyl chain.[6] Type **A** rigid rods with short carbyne bridge (k = 1/2 and 1) were obtained through a metathesis reaction between $[Ru_2(ap)_4]Cl$ and $Li(CC)_{2k}Li$.[6] Analogous rods with $2k \geq 4$ can be obtained by homocoupling of $[Ru_2(ap)_4](C_{2k}H)$ (**C** in Scheme 1), a monofunctional building block established in our laboratory,[7,8] under either Hay or Eglington conditions.[9,10] To extend our scope into the monodisperse oligomer (**B**, Scheme 1), difunctional building block **D** (Scheme 1) is necessitated from structural considerations. Examples of this type of building block, *trans*-$[Ru_2(ap)_4](C_4SiMe_3)_2$ and *trans*-$[Ru_2(DmAniF)_4](C_4SiMe_3)_2$ (*DmAniF* is di(*m*-methoxyphenylformamidinate)), have also been established in our[8,11] and Lehn's laboratories.[12] Reported herein are the synthesis and characterization of a family

Scheme 1. Retrosyntheses of Both Simple Rod with $[Ru_2]$ Terminus (A) and Oligometallayne Rod (B) from Synthons C and D; $[Ru_2] = [Ru_2(ap)_4]$

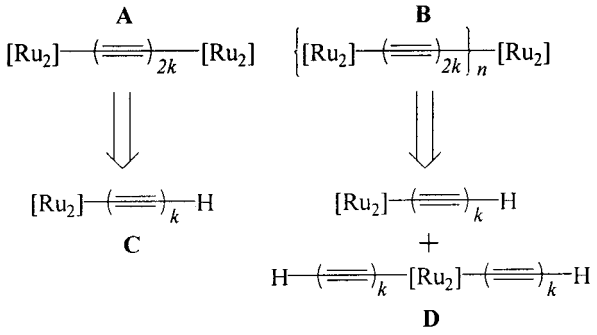

* Tel: (305) 284-6617. Fax: (305) 284-1880. E-mail: tren@miami.edu.

(1) Mullen, K.; Wegner, G. *Electronic Materials: the Oligomer Approach*; Wiley-VCH: Weinheim, 1998.
(2) Geerts, Y.; Klarner, G.; Mullen, K. In *Electronic Materials: the Oligomer Approach*; Mullen, K., Wegner, G., Eds.; Wiley-VCH: Weinheim, 1998.
(3) Schumm, J. S.; Pearson, D. L.; Tour, J. M. *Angew. Chem., Int. Ed. Engl.* **1994**, *33*, 1360.
(4) Tour, J. M. *Chem. Rev.* **1996**, *96*, 537.
(5) Moore, J. S. *Acc. Chem. Res.* **1997**, *30*, 402.
(6) Ren, T.; Zou, G.; Alvarez, J. C. *Chem. Commun.* **2000**, 1197.
(7) Zou, G.; Alvarez, J. C.; Ren, T. *J. Organomet. Chem.* **2000**, *596*, 152.
(8) Xu, G.; Ren, T. *Organometallics* **2001**, *20*, 2400.
(9) Ni, Y.; Ren, T. *Angew. Chem., Int. Ed.*, manuscript in preparation.
(10) Siemsen, P.; Livingston, R. C.; Diederich, F. *Angew. Chem., Int. Ed.* **2000**, *39*, 2632.
(11) Xu, G.; Ren, T. *Inorg. Chem.* **2001**, *40*, 2925.
(12) Wong, K.-T.; Lehn, J.-M.; Peng, S.-M.; Lee, G.-H. *Chem. Commun.* **2000**, 2259.

10.1021/om0109004 CCC: $22.00
Publication on Web 01/19/2002

Scheme 2. Ethynyl and Ethynyl-Butadinyl Adducts on the $[Ru_2(ap)_4]$ Core

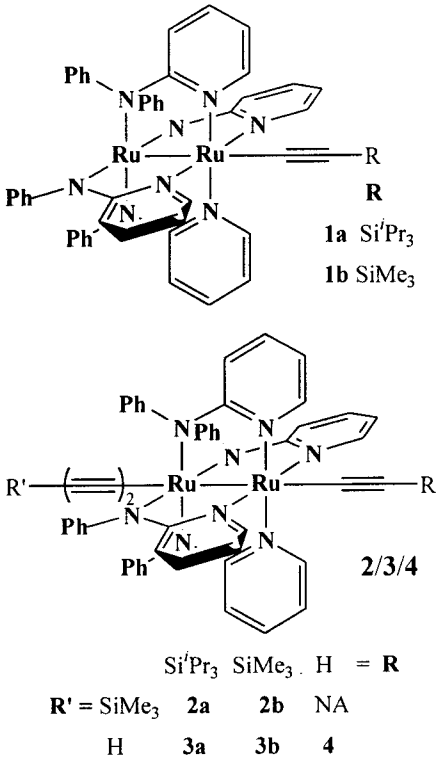

Scheme 3. Stepwise Formation of Mono- and Bis-butadiynyl adducts on $[Ru_2(ap)_4]$

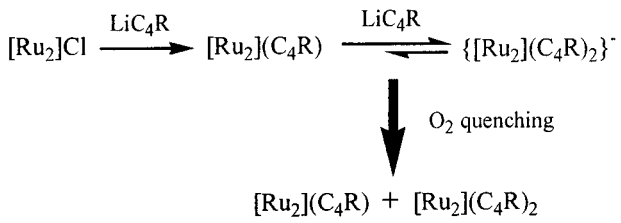

of dissymmetric ethynyl-butadiynyl adducts on the $[Ru_2(ap)_4]$ core, illustrated in Scheme 2, which not only satisfy the structural requirement for a type **D** building block but also exhibit selective desilylation chemistry to yield two compounds (**3a**/**3b**) that are amenable to the divergent−convergent synthesis.

Results and Discussion

It was demonstrated previously that monoethynyl adduct $[Ru_2(ap)_4](C_2R)$ was the only product isolated when treating $Ru_2(ap)_4Cl$ with either 1 equiv or excess lithiated ethynyl ligand (LiC_2R).[7,8,13] However, replacing the ethynyl ligand with a longer butadiynyl ligand enabled the isolation of the bis-adduct *trans*-$[Ru_2(ap)_4](C_4R)_2$ (R = $SiMe_3$) in addition to the monoadduct when excess LiC_4R was used.[8] Evidently, the addition of butadiynyl ligands to $[Ru_2(ap)_4]$ core proceeds stepwise, as described in Scheme 3.

In the case of ethynyl ligands, the second addition step is prohibited by the steric repulsion between the R and anilino groups. On the other hand, a dissymmetrical adduct may be expected if the monoethynyl adduct is treated with a longer poly-ynyl ligand such as butadiynyl.

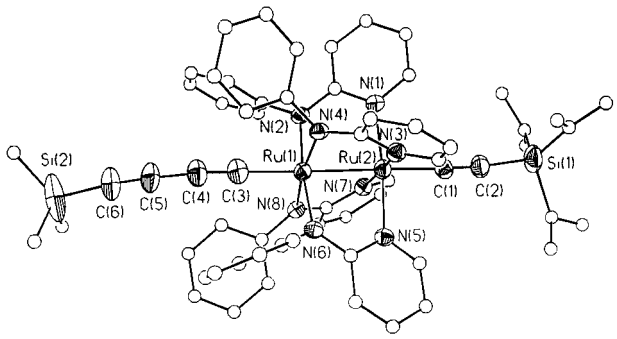

Figure 1. ORTEP plot of molecule **2a** at 30% probability level. All non-acetylenic carbons are shown as isotropic atoms.

Similar to the synthesis of $[Ru_2(ap)_4]C_2SiMe_3$ (**1b**),[7] $[Ru_2(ap)_4]C_2Si^iPr_3$ (**1a**) was prepared by treating $[Ru_2(ap)_4]Cl$ with 1 equiv of $LiC_2Si^iPr_3$ and the yield was quantitative. When **1a** was treated with 6 equiv of LiC_4SiMe_3 under inert atmosphere, the initially green solution gradually changed to dark red, a color likely attributed to $\{trans\text{-}(R'C_4)[Ru_2(ap)_4](C_2R)\}^{-1}$. The aliquot of reaction mixture turned to dark blue instantly upon exposure to air, and TLC analysis revealed the formation of a dominant blue product and the presence of **1a**. After ca. 3 h, the ratio between the blue product and **1a** became constant on TLC plate, and the reaction was terminated by bubbling O_2 through the reaction mixture, which led to a royal blue solution in minutes. Compound **2a** was isolated in satisfactory yield (76%) after the chromatography purification of reaction mixture. Starting with **1b**, compound **2b** was prepared similarly in good yield (77%).

The Me_3Si group in compound **2a** can be readily removed with the weak base K_2CO_3 to yield **3a** in 24 h, and the process is shortened to 30 min by using the strong base NaOH. In either case, there was no evidence of the removal of the Si^{i}Pr$_3$ group. When treated with K_2CO_3, the Me_3Si group of the butadiynyl ligand in **2b** was completely removed in 48 h, and partial removal of the second Me_3Si group to yield compound **4** was noticed. Removal of both Me_3Si groups in **2b** was accomplished by using the strong base NaOH, where the conversion of **2b** to **3b** completed within 30 min, and the subsequent conversion of **3b** to **4** finished in 24 h. The sequential deprotection of Me_3Si groups in **2b** clearly indicates that they are electronically differentiated. A plausible explanation is that the carbon ends of the $C_4-Ru_2-C_2$ backbone are electronically communicating due to full conjugation.

Compound **1a** has a room-temperature effective magnetic moment of 4.11, indicating a $S = 3/2$ ground state that was observed for **1b** as well.[7] Compounds **2**, **3**, and **4** are diamagnetic, as reflected by the well-resolved ^1H NMR spectra.

Molecular structures determined via X-ray diffraction studies are shown in Figures 1 and 2 for **2a** and **3b**, respectively, and the selected metric parameters are presented in Table 1. Clearly, the *ap* bridging ligands in both structures retain the (4,0)-arrangement common to all $[Ru_2(ap)_4]$-based alkynyl compounds:[7,8,13] all py-

(13) Chakravarty, A. R.; Cotton, F. A. *Inorg. Chim. Acta* **1986**, *113*, 19.

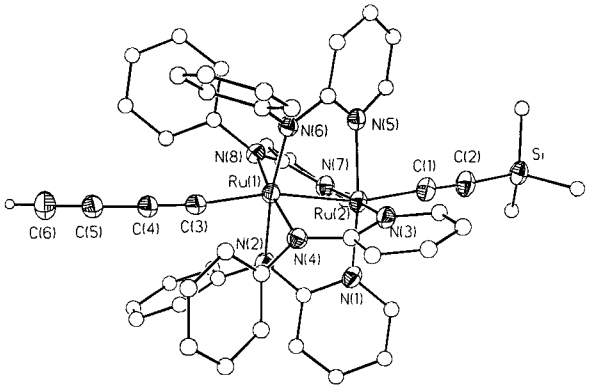

Figure 2. ORTEP plot of molecule **3b** at 30% probability level. All non-acetylenic carbons are shown as isotropic atoms.

Table 1. Selected Bond Lengths and Angles for Molecules 2a and 3b

	2a	**3b**
Ru(1)−Ru(2)	2.4584(6)	2.4662(3)
Ru(1)−N(2)	2.038(3)	2.142(2)
Ru(1)−N(4)	2.075(4)	2.025(2)
Ru(1)−N(6)	2.036(3)	1.968(2)
Ru(1)−N(8)	2.039(4)	2.035(2)
Ru(2)−N(1)	2.060(4)	1.999(2)
Ru(2)−N(3)	2.049(4)	2.080(2)
Ru(2)−N(5)	2.082(4)	2.156(2)
Ru(2)−N(7)	2.101(4)	2.044(2)
Ru(2)−C(1)	1.969(5)	1.972(3)
C(1)−C(2)	1.193(6)	1.214(4)
Si(1)−C(2)	1.833(6)	1.812(3)
Ru(1)−C(3)	1.963(6)	1.966(3)
C(3)−C(4)	1.202(7)	1.206(4)
C(4)−C(5)	1.399(8)	1.370(4)
C(5)−C(6)	1.200(7)	1.175(5)
Si(2)−C(6)	1.794(6)	NA
N(2)−Ru(1)−Ru(2)	85.89(10)	78.02(6)
N(4)−Ru(1)−Ru(2)	83.55(10)	86.60(6)
N(6)−Ru(1)−Ru(2)	87.19(10)	93.51(6)
N(8)−Ru(1)−Ru(2)	88.84(10)	85.55(6)
N(1)−Ru(2)−Ru(1)	87.99(11)	94.71(7)
N(3)−Ru(2)−Ru(1)	89.68(11)	86.05(6)
N(5)−Ru(2)−Ru(1)	86.74(10)	78.89(6)
N(7)−Ru(2)−Ru(1)	84.68(10)	87.33(6)
C(1)−Ru(2)−Ru(1)	175.12(15)	165.31(9)
C(2)−C(1)−Ru(2)	177.1(5)	175.2(3)
C(3)−Ru(1)−Ru(2)	177.74(17)	164.84(8)
C(4)−C(3)−Ru(1)	172.6(5)	173.1(3)
C(3)−C(4)−C(5)	172.7(6)	172.7(3)
C(6)−C(5)−C(4)	176.9(8)	177.2(4)

ridine *N*-centers coordinate to Ru(2), while all anilino *N*-centers coordinate to Ru(1). The Ru−Ru bond lengths in **2a** (2.4584(6) Å) and **3b** (2.4662(3) Å) are consistent with a formal Ru−Ru single bond. Four chemically distinct Ru−C_α distances in molecules **2a** and **3b** are identical within experimental error and a mean of 1.968-[4] Å. The C−C bond lengths of ethynyl-butadiynyl ligands in **2a** and **3b** are comparable, and those of butadiynyls generally conform to the alternating single and triple bond formalism.

Close examination of structures of **2a** and **3b** reveals that neither molecule has a perfectly linear C_4−Ru_2−C_2 backbone. The deviation of the Ru−Ru−C angles from linearity is largely attributed to a second-order Jahn−Teller distortion that is common to *trans*-bis-(alkynyl) adducts on a Ru_2(III,III) core.[14] This effect is very pronounced in **3b**, as indicated by the great disparity in Ru−N bond lengths. More specifically, the

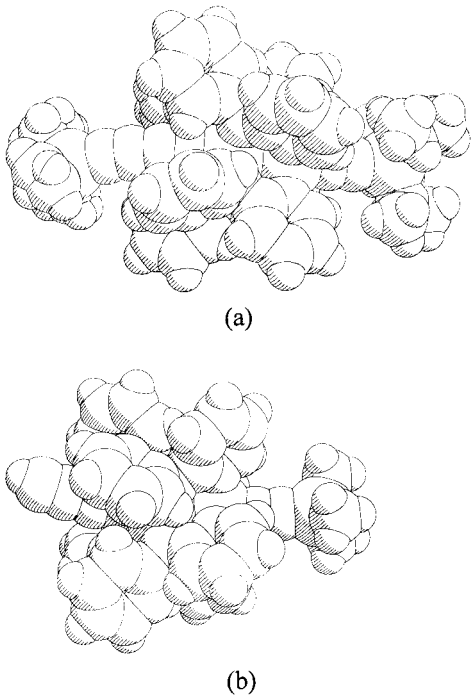

Figure 3. Space-filling plots of molecules **2a** (a) and **3b** (b).

Ru(1)−N(2) bond (2.142(2) Å) is 0.1 Å longer than the mean of Ru(1)−N bonds (2.043 Å), while the bond *trans* to it, Ru(1)−N(6), is only 1.968(2) Å long. Similar distortions occur on the Ru(2) center: elongation of the Ru(2)−N(5) bond and compression of the Ru(2)−N(1) bond. In comparison, the distortion of Ru−N bonds in **2a** is relatively subtle, with the largest deviation from the mean (2.06 Å) in Ru(2)−N(7) (2.101(4) Å). Variation in the degree of distortion is also apparent in bond angles: the Ru−Ru−C_α angles in **2a** (175.12(15)° and 177.74(17)°) are very close to 180°, but those in **3b** (165.31(9)° and 164.84(8)°) are ca. 15° away from linearity. Inspection of the space-filling plots of both **2a** and **3b** (Figure 3) reveals that the Si^iPr_3 group fully occupies the space around the acetylenic bond and leaves little space for the Ru−C_α bond to bend, while the same steric restraint is unavailable from the $SiMe_3$ group in **3b**. It is plausible that the bulkiness of the Si^iPr_3 group suppresses the second-order Jahn−Teller effect in **2b**.

Similar to compound **1b** reported earlier,[7] compound **1a** exhibits two reversible one-electron processes in its cyclic voltammogram (CV) shown in Figure 4: an oxidation at 0.455 V and a reduction at −0.877 V. Cyclic voltammograms recorded at the scan rate of 0.100 V/s for bis-alkynyl adducts, compounds **2a**/**b**, **3a**/**b**, and **4** are also shown in Figure 4, and they appear more complicated in comparison with that of **1a**. The main features of the CVs of **2a**/**b** consist of three one-electron couples: an oxidation (ca. 0.830 V, **A**), the first reduction (−0.365 V, **B**), and the second reduction (−1.480 V, **C**). These couples have been respectively shifted by ca. −0.06, −0.08, and −0.12 V from that of *trans*-[Ru_2(*ap*)$_4$]-(C_4SiMe_3)$_2$,[8] which are attributed to the slight electron-richness of both **2a** and **2b** in comparison with *trans*-

(14) Lin, C.; Ren, T.; Valente, E. J.; Zubkowski, J. D. *J. Chem. Soc., Dalton Trans.* **1998**, 571.

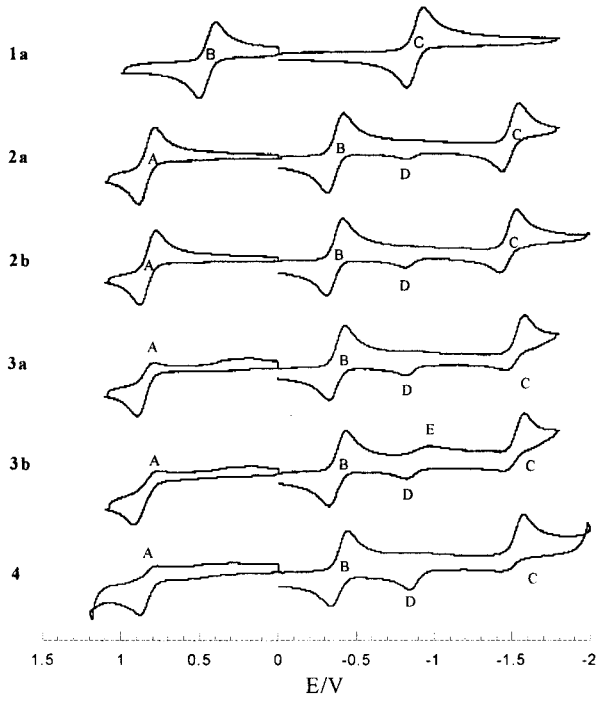

Figure 4. Cyclic voltammograms of compounds **1**−**4** recorded in 0.20 M THF solution of Bu_4NPF_6 at a scan rate of 0.10 V/s.

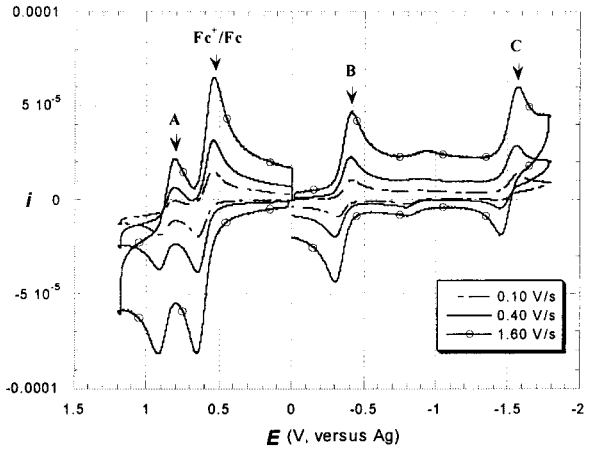

Figure 5. Cyclic voltammograms of compound **3a** recorded in 0.20 M THF solution of Bu_4NPF_6 at scan rates of 0.10, 0.40, and 1.60 V/s (see legend). A silver wire was used as a pseudo-reference electrode, and ferrocene was added as the internal reference.

$[Ru_2(ap)_4](C_4SiMe_3)_2$. While the first two couples of **2** are reversible, the latter has an $i_{backward}/i_{forward}$ ratio equal or less than 0.70 and, hence, is quasi-reversible. Both compounds **2a**/**b** also display a small but significant wave around −0.820 V (**D**) during the backward sweeping of cathodic scan.

For both partially and fully desilylated compounds, i.e., **3a**/**b** and **4**, their CVs also feature three couples, an irreversible oxidation (**A**), a reversible reduction (**B**), and an irreversible reduction (**C**). Clearly, the redox stability of bis-alkynyl adducts is reduced significantly upon desilylation. Coupled with the disappearance of the anodic wave of couple **C**, the wave at ca. −0.820 V (**D**) becomes very pronounced. On the other hand, the backward sweep of the anodic scan reveals the superposition of many featureless small waves.

Rationales for the observed redox characteristics are summarized in Scheme 4. Electrochemically generated dianions are relatively unstable and dissociate the butadiynyl anion on the electrochemical time scale to yield the monoalkynyl complex anion, which was oxidized to yield wave **D**. This assignment is readily verified by noticing that E_{pa}(**D**) is about the same as the E_{pa} of the reduction couple of **1a**. Dissociation upon reduction is not limited to the dianion: a small but significant $i_{forward}$ has been observed at the potential corresponding to $E_{pc}(0/-1)$ of **1a** for both **3b** and **4** (marked as **E** in the CV of **3b**), which indicates the partial dissociation of the butadiynyl anion upon the formation of monoanion. The irreversibility of the oxidation couple (**A**) is associated with the desilylation of butadiynyl, as evidenced by the contrast between the CVs of **2a**/**b** and **3a**/**3b**. However, the fate of the cation remains unclear presently.

It was noted for compounds **3a**/**3b** and **4** that the reversibility of both **A** and **C** couples improves upon the increase in scan rate from 0.10 V/s. Due to the instability of the Ag/AgCl reference electrode (Cypress) at higher scan rates, a silver wire pseudo-reference electrode was used and the potential was calibrated with ferrocene as the internal standard. The dependence of reversibility on scan rate is typified by the CVs of **3a** shown in Figure 5, where the oxidation couple (**A**) becomes reversible and the second reduction couple (**C**) becomes quasi-reversible with scan rate higher than 1 V/s. Similar results were obtained for compounds **3b** and **4**, and all the rate-dependent results are provided as Supporting Information (Tables S9−S11).

Compounds **1**−**4** display rich features in their vis−NIR (visible−near-infrared) spectra, as shown in Figure 6. Compound **1a** has two intense peaks centered at 471 and 745 nm, respectively, which are similar to these observed for both $Ru_2(ap)_4Cl$[15] and $Ru_2(ap)_4(CCR)$ (R = H, Ph, CH_2OCH_3).[7,13] The low-energy absorption can be attributed to the π(Ru−N) to $\pi^*/\delta^*(Ru_2)$ charge-transfer band, while the high-energy band is likely associated with $\pi(CCR)$ to $\pi^*/\delta^*(Ru_2)$.[13,16] It is interesting to note that the HOMO−LUMO gap (ΔE) of solvated **1a** is estimated to be 1.332 eV from voltammetric data ($\Delta E = e\{E_{1/2}(+1/0) - E_{1/2}(0/-1)\}$)[17,18] and 1.664 eV from

Scheme 4. Assignment of Redox Couples and Related Chemical Steps

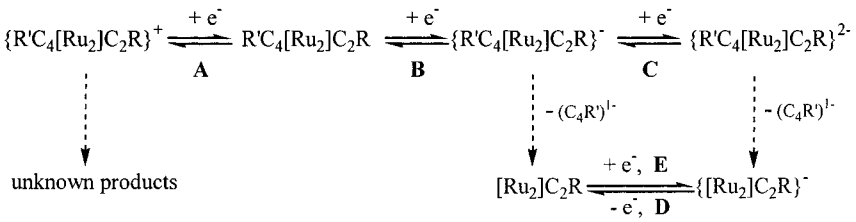

Table 2. Electrochemical and Spectroscopic Data for Compounds 1−4

	1b	2a	2b	3a	3b	4
$E(+1/0)$/V	0.455	0.835	0.827	0.843[a]	0.834[a]	0.830[a]
(ΔE_p/V, $i_{back}/i_{forward}$)	(0.103, 0.99)	(0.102, 0.88)	(0.099, 0.90)			
$E(0/-1)$/V	−0.877	−0.370	−0.362	−0.380	−0.378	−0.390
(ΔE_p/V, $i_{back}/i_{forward}$)	(0.109, 0.96)	(0.100, 1.00)	(0.104, 0.86)	(0.101, 1.01)	(0.100, 1.15)	(0.102, 1.12)
$E(-1/-2)$/V	NA	−1.493	−1.476	−1.539[a]	−1.514[a]	−1.527[a]
(ΔE_p/V, $i_{back}/i_{forward}$)		(0.098, 0.72)	(0.102, 0.61)			
λ_{max}/nm (ϵ, $cm^{-1}M^{-1}$)	471 (8000)	440 (sh)	440 (sh)	437 (3870)	435 (6140)	435 (8530)
	745 (5700)	480 (5300)	480 (9600)	476 (4650)	477 (6430)	477 (9050)
		656 (7500)	655 (13 700)	644 (6500)	645 (10 700)	644 (14 950)
		1040 (4600)	1040 (8450)	1035 (3970)	1035 (6580)	1029 (9090)
$\{E(+1/0) - E(0/-1)\}$/V	1.332	1.206	1.209	1.223	1.212	1.220
E_{op}, eV[b]	1.66	1.19	1.19	1.20	1.20	1.21

[a] These couples are irreversible at the scan rate of 0.10 V/s; $E_{1/2}$ values listed were averaged from those obtained at higher scan rates. [b] $E_{op} = 10^7/(8065.5\lambda_{max})$.

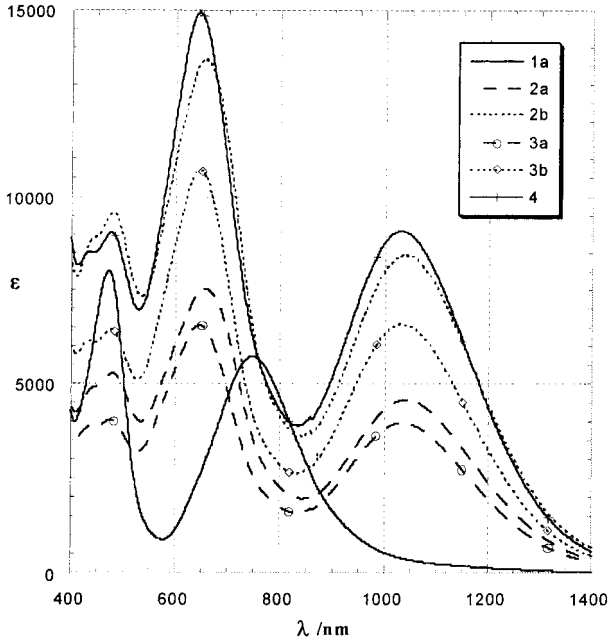

Figure 6. Vis−NIR absorption spectra of compounds **1**−**4** recorded in THF.

the λ_{max} (745 nm). The discrepancy is perhaps related to the open-shell nature of **1a**.

As shown in Figure 6, bis-alkynyl species **2**−**4** exhibit more intense peaks, which are generally shifted to longer wavelengths in comparison with those of **1a**. The lowest energy charge-transfer bands appear around 1035 nm, which is assigned as the π(Ru−N) to $\pi^*/\delta^*(Ru_2)$ charge-transfer band. The dramatic red-shift from that of **1** can be attributed to the decrease in the energies of $\pi^*/\delta^*(Ru_2)$ orbitals upon the increase in formal oxidation state (Ru_2(III,III) in **2**−**4** versus Ru_2-(II,III) in **1**). The intense peaks at ca. 650 and 480 nm, which were also observed for *trans*-$[Ru_2(ap)_4](C_4SiMe_3)_2$,[8] are tentatively assigned as $\pi(CCR)$ to $\pi^*/\delta^*(Ru_2)$ transitions. Compounds **2**−**4** also exhibit an additional peak/shoulder around 440 nm that is likely due to the dissymmetric nature of **2**−**4** since such a peak was absent in *trans*-$[Ru_2(ap)_4](C_4SiMe_3)_2$.

The most noteworthy feature of compounds **2**−**4** is the small HOMO−LUMO gap, which is around 1.20 eV from both electrochemical and optical data (see Table 2). The value of 1.20 eV is remarkably small for organometallic species that are stable toward both air and moisture. Since the reduction of the HOMO−LUMO gap has been the primary goal of band gap engineering of the conjugated oligomer/polymer,[19,20] it is very important to understand the electronic nature of compounds **2**−**4** on the basis of first-principles calculations, which are being carried out in our group.

Conclusions

Several dissymmetric ethynyl-butadiynyl adducts on $[Ru_2(ap)_4]$ core have been synthesized, and they display rich redox chemistry and spectroscopic features. Most significantly, the monodesilylated compounds **3a**/**b** can be readily synthesized due to the electronic asymmetry. With these orthogonally protected building blocks, one can envision the divergent−convergent synthesis of monodisperse oligomers outlined in Scheme 5, which is being vigorously pursued in our laboratory.

Scheme 5. Divergent−Convergent Coupling of Ru_2-metalla-yne

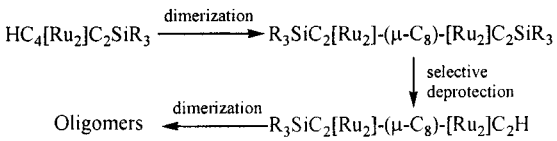

Experimental Section

Tri(isopropyl)silylacetylene, 1,4-bistrimethylsilyl-1,3-butadiyne, 2-anilinopyridine, and *n*-BuLi were purchased from Aldrich, and silica gel was purchased from Merck. Both $Ru_2(ap)_4Cl$ and $Ru_2(ap)_4(CCSiMe_3)$ (**1b**) were prepared as previously described.[7] THF was distilled over Na/benzophenone under an N_2 atmosphere prior to use. ^1H and ^{13}C NMR spectra were recorded in $CDCl_3$ (except **4**) on a Bruker AVANCE300 NMR spectrometer, and chemical shifts (δ) were respectively referenced to the residual $CHCl_3$ and the solvent $CDCl_3$. Infrared spectra were recorded on a Perkin-Elmer 2000 FT-IR spectrometer using KBr disks. UV−vis spectra in THF were obtained with a Perkin-Elmer Lambda-900 UV−vis spectrophotometer. Magnetic susceptibility was measured at 293 K with a Johnson Matthey Mark-I Magnetic Susceptibility

(15) Chakravarty, A. R.; Cotton, F. A.; Tocher, D. A. *Inorg. Chem.* **1985**, *24*, 172.
(16) Miskowski, V. M.; Hopkins, M. D.; Winkler, J. R.; Gray, H. B. In *Inorganic Electronic Structure and Spectroscopy*; Solomon, E. I., Lever, A. B. P., Eds.; Wiley: New York, 1999; Vol. 2.
(17) Ren, T. *Coord. Chem. Rev.* **1998**, *175*, 43.
(18) Loutfy, R. O.; Loutfy, R. O. *Can. J. Chem.* **1976**, *54*, 1454.
(19) Roncali, J. *Chem. Rev.* **1997**, *97*, 173.
(20) van Mullekom, H. A. M.; Vekemans, J.; Havinga, E. E.; Meijer, E. W. *Mater. Sci. Eng. R−Rep.* **2001**, *32*, 1.

Balance. Cyclic voltammograms (CV) were recorded in 0.20 M (n-Bu)$_4$NPF$_6$ solution (THF, N_2-degassed) on a CHI620A voltammetric analyzer with a glassy carbon working electrode ($\Phi = 3$ mm), a Pt wire auxiliary electrode, and a concentration of diruthenium species about 1.0 mM. For the CV shown in Figure 4 (all with a scan rate of 0.10 V/s), a Ag/AgCl reference electrode for nonaqueous solution (Cypress) was used and the ferrocenium/ferrocene couple was observed at 0.576 V under the experimental conditions. However, responses of the Ag/AgCl reference electrode became sluggish at higher scan rate. Hence, a Ag wire pseudo-reference electrode was used for the scan-rate dependence study of compounds **3** and **4**, and the potentials reported were calibrated with ferrocene as the internal standard.

Preparation of Ru$_2$(ap)$_4$(C$_2$Si^{i}Pr$_3$) (1a). To a 20 mL THF solution containing 1.2 mmol of ^{i}Pr$_3$SiC$_2$H was added 0.80 mL of BuLi (1.6 M in hexanes) at −80 °C. The mixture was slowly warmed to room temperature and stirred for another hour to yield a light yellow solution. All the solution was transferred to a flask containing a THF solution (100 mL) of Ru$_2$(ap)$_4$Cl (0.98 g, 1.05 mmol). The solution color changed from dark green to yellow-green gradually, and the reaction mixture was stirred for an hour. Removal of the solvents in vacuo yielded a green residue, which was rinsed with a copious amount of warm methanol and filtered. A light green flaky crystalline solid was obtained after drying in a vacuum and identified as pure **1a**. Yield: 1.07 g (96%). Data for **1a**: R_f, 0.88 (Et$_3$N/ethyl acetate/hexanes, 1/1/10, v/v, and the same solvent combination was used for all the R_f values thereafter). Anal. for C$_{55}$H$_{57}$N$_8$SiRu$_2$, found (calcd): C, 62.13 (62.30); H, 5.53 (5.42); N, 10.39 (10.57). MS-FAB (*m/e*, based on ^{101}Ru): 1061 [MH$^+$]. IR: ν(C ≡ C)/cm^{-1}, 1993(w). Magnetic (293 K): χ_{mol}(corr): 7.20×10^{-3} esu·mol^{-1}. μ_{eff}: 4.11 μ_B.

Preparation of *trans*-(4,0)-(Me$_3$SiC$_4$)[Ru$_2$(ap)$_4$](C$_2$Si^{i}Pr$_3$) (2a). To a 30 mL THF solution containing 3.0 mmol of Me$_3$SiC$_4$SiMe$_3$ was added 1.9 mL of n-BuLi (1.6 M in hexanes) at −80 °C. The mixture was slowly warmed to room temperature and stirred for 2 h to yield a light yellow solution. The solution was transferred to a flask containing a THF solution (35 mL) of Ru$_2$(ap)$_4$(C$_2$Si^{i}Pr$_3$) (0.53 g, 0.50 mmol). The solution color changed from dark green to reddish purple over a period of an hour, and the reaction mixture was stirred for an additional 2 h. The reaction was terminated by bubbling dry O_2 through the solution, which turned dark blue immediately. TLC analysis (Et$_3$N/ethyl acetate/hexanes, 1/1/10, v/v) revealed the presence of starting material **1** (<10%), **2a** (dominant), and **3a** (trace). After the solvent removal, the dark residue was loaded onto a silica gel column deactivated by 1% Et$_3$N in hexanes and eluted with a linear gradient of Et$_3$N/ethyl acetate/hexanes (1/0/100 to 1/10/100, v/v). Removal of solvents in the blue fraction resulted in **2a** as a dark blue polycrystalline solid (450 mg, 76% based on Ru). Data for **2a**: R_f 0.81. Anal. for C$_{62}$H$_{66}$N$_8$Si$_2$Ru$_2$, found (calcd): C, 63.34 (63.02); H, 5.84 (5.63); N, 9.27 (9.48). MS-FAB (*m/e*, based on ^{101}Ru): 1182 [M$^+$]. ^{1}H NMR: 9.33 (q, 4H, aromatic), 7.04 (m, 4H, aromatic), 6.98 (m, 12H, aromatic), 6.39 (d, 4H, aromatic), 6.29 (t, 4H, aromatic), 5.72 (s, 8H, aromatic), 1.23 (br, 21H, *i*-Pr) 0.12 (s, 9H, Si(C*H*$_3$)$_3$). ^{13}C NMR (C≡C, all singlet): 109.6, 104.6, 74.1, 73.9, 73.7, 73.3, IR: ν(C ≡ C)/cm^{-1}, 1999(s), 2110(s), and 2173(w).

Preparation of *trans*-(4,0)-(HC$_4$)[Ru$_2$(*ap*)$_4$](C$_2$Si^{i}Pr$_3$) (3a). 2a (0.40 g) was dissolved in 150 mL of THF/MeOH (2/1 v/v) to which was added 4.0 g of NaOH. The mixture was stirred vigorously, and **2a** was cleanly converted to **3a** in 30 min (monitored by TLC). After removal of solvent, compound **3a** was extracted using CH_2Cl_2 and the extract was rinsed thoroughly with water. The residue after solvent removal was recrystallized from hexanes/CH_2Cl_2 to yield blue crystalline **3a** (0.35 g, 93%). Treating **2a** with K_2CO_3 under similar conditions also produced **3a** in good yield, but the reaction time was longer (24 h). Data for **3a**: R_f 0.67. Anal. for C$_{59}$H$_{58}$N$_8$SiRu$_2$, found (calcd): C, 63.60 (63.88); H, 5.60(5.27); N, 9.81-(10.10). MS-FAB (*m/e*, based on ^{101}Ru): 1110 [MH$^+$]. ^{1}H NMR: 9.34 (q, 4H, aromatic), 7.01−7.11 (m, 16H, aromatic), 6.43 (d, 4H, aromatic), 6.32 (dd, 4H, aromatic), 5.76 (d, 8H, aromatic), 1.22 (br, 21H), 1.09 (s, 1H, C$_4$*H*). ^{13}C NMR (C≡C, all singlet): 109.5, 104.6, 74.2, 73.9, 73.7, 73.3. IR: ν(C ≡ C)/cm^{-1}, 1989(s) and 2133(s).

Preparation of *trans*-(MeSi$_3$C$_4$)Ru$_2$(*ap*)$_4$(C$_2$SiMe$_3$) (2b). Similar to the preparation of **2a**, Ru$_2$(ap)$_4$(C$_2$SiMe$_3$)[7] (**1b**, 0.40 g, 0.41 mmol) was treated with 2.45 mmol of LiC$_4$SiMe$_3$ in THF. After a similar workup, **2b** was isolated as a blue crystalline powder (0.35 g, 77% based **1b**). Data for **2b**: R_f, 0.81. Anal. for C$_{56}$H$_{54}$N$_8$Si$_2$Ru$_2$, found (calcd): C, 60.99 (61.29); H, 4.92 (4.96); N, 10.29 (10.21). MS-FAB (*m/e*, based on ^{101}Ru): 1098 [MH$^+$]. ^{1}H NMR: 9.26 (q, 4H, aromatic), 7.11 (m, 4H, aromatic), 7.03 (m, 12H, aromatic), 6.35−6.46 (m, 8H, a romatic), 5.77 (s, 8H, aromatic), 0.37 (s, 9H, C*H*$_3$), 0.18 (s, 9H, C*H*$_3$). ^{13}C NMR (C≡C, all singlet): 109.7, 104.8, 74.2, 73.9, 73.7, 73.3. IR: ν(C ≡ C)/cm^{-1}, 1998(s), 2117(s), and 2180(w).

Preparation of *trans*-(HC$_4$)Ru$_2$(*ap*)$_4$(C$_2$SiMe$_3$) (3b). Compound **2b** (150 mg) was stirred with 7 g of K_2CO_3 in 50 mL of THF/MeOH (2/1) solution for 48 h when TLC analysis indicated the complete disappearance of **2b**. The solution was filtered, and the filtrate was loaded onto silica and eluted with Et$_3$N/ethyl acetate/hexanes (1/10/90, v/v). Compound **3b** was isolated as a blue crystalline solid (120 mg, 86%). A Trace amount of **4** (<10%) was also present. Data for **3b**: R_f, 0.65. Anal. for C$_{53}$H$_{46}$N$_8$SiRu$_2$, found (calcd): C, 62.12 (62.09); H, 4.58 (4.52); N, 10.65 (10.93). MS-FAB (*m/e*, based on ^{101}Ru): 1026 [MH$^+$]. ^{1}H NMR: 9.20 (q, 4H, aromatic), 7.00−7.10 (m, 16H, aromatic), 6.42 (d, 4H), 6.39 (t, 4H, aromatic), 5.75 (d, 8H, aromatic), 1.09 (s, 1H, C$_4$*H*), 0.31 (s, 9H, Si(C*H*$_3$)$_3$). ^{13}C NMR (C≡C, all singlet): 109.6, 104.9, 74.2, 73.9, 73.7, 73.3. IR: ν(C ≡ C)/cm^{-1}, 1996(s) and 2129(s).

Preparation of *trans*-(HC$_4$)Ru$_2$(ap)$_4$(C$_2$H) (4). Compound **2b** (120 mg) was dissolved in 40 mL of THF to which was added 6.0 g of NaOH and 20 mL of MeOH. Starting material was completely converted to **3b** and **4** within 30 min, and the remaining **3b** was converted to **4** after 24 h vigorous stirring. Some purple polar materials also appeared toward the end of the reaction, which have not been identified yet. After solvent removal, the dark blue jelly residue was dissolved in CH_2Cl_2 and washed with a copious amount of water until the washing became neutral. The CH_2Cl_2 solution was loaded onto silica and eluted with Et$_3$N/ethyl acetate/hexanes (1/10/100 to 1/40/40), yielding pure **4** as blue microcrystalline solids. Yield: 0.090 g (81%). Data for **4**: R_f, 0.40. Anal. for C$_{50}$H$_{41}$N$_8$O$_{1.5}$Ru$_2$ (**4**·1.5H$_2$O), found (calcd): C, 61.60 (61.38); H, 4.30 (4.22); N, 11.17 (11.43). MS-FAB (*m/e*, based on ^{101}Ru): 954 [MH$^+$]. ^{1}H NMR((CD$_3$)$_2$CO): 9.20 (d, 4H, aromatic), 7.00−7.10, (m, 16H), 6.36−6.44 (m, 8H), 5.75 (d, 8H, aromatic), 5.27 (s, 1H), and 2.91 (s, 1H). ^{13}C NMR (C$_6$D$_6$; C≡C, all singlet): 109.8, 104.9, 64.0, 61.8, 60.4. IR: ν(C≡C)/cm^{-1}, 1943(w) and 2121(s).

X-ray Data Collection, Processing, and Structure Analysis and Refinement. Single crystals of both compounds **2a** and **3b** were grown via slow evaporation of the fractions of column purification. The X-ray intensity data were measured at 300 K on a Bruker SMART1000 CCD-based X-ray diffractometer system using Mo Kα radiation (λ = 0.71073 Å). Crystals used for X-ray crystallographic analysis were cemented onto a quartz fiber with epoxy glue. Data were measured using omega scans of 0.3° per frame such that a hemisphere (1271 frames) was collected. No decay was indicated for either data set by the re-collection of the first 50 frames at the end of each data collection. The frames were integrated with the Bruker SAINT software package using a narrow-frame integration algorithm,[21] which also corrects for the Lorentz and polarization effects. Absorption corrections were applied using SADABS supplied by George Sheldrick.

(21) *SAINT V 6.035 Software for the CCD Detector System*; Bruker-AXS Inc., 1999.

Table 3. Crystal Data for Compounds 2a and 3b

	2a	**3b**
formula	$C_{62}H_{66}N_8Si_2Ru_2$	$C_{53}H_{46}N_8SiRu_2$
fw	1181.6	1025.2
space group	$P\bar{1}$ (No. 2)	$P2_1/c$ (No. 14)
a, Å	10.533(1)	14.203(1)
b, Å	16.089(2)	14.954(1)
c, Å	19.641(2)	22.605(1)
α, deg	69.229(2)	90
β, deg	88.810(2)	93.576(1)
γ, deg	72.410(2)	90
V, Å^3	2952.5(6)	4791.6(5)
Z	2	4
$\rho_{calc.}$, g cm^{-3}	1.329	1.421
μ, mm^{-1}	0.597	0.700
λ(Mo Kα), Å	0.71073	0.71073
T, °C	27	27
no. of reflns collected	15 686	25 242
no. of ind reflns	10 270 [R(int) = 0.0246]	8428 [R(int) = 0.0238]
final R indices [$I > 2\sigma(I)$]	R1 = 0.0481, wR2 = 0.0969	R1 = 0.0282, wR2 = 0.0594

The structures were solved and refined using the Bruker SHELXTL (Version 5.1) software package in the space groups $P\bar{1}$ and $P2_1/c$ for crystals **2a** and **3b**, respectively.[22−24] Positions of all non-hydrogen atoms of diruthenium moieties were revealed by direct methods. In both cases, the asymmetric unit contains one diruthenium molecule. The methyl carbon atoms of the $SiMe_3$ group in **2a** are disordered over two positions and were refined with occupancy and distance constraints. The H6 atom in **3b**, the terminal hydrogen of the butadiynyl ligand, was located from the difference map and refined freely, while the positions of all other hydrogen atoms were calculated. Both structures were refined to convergence by least-squares method on F^2, SHELXL-93, incorporated in SHELXTL.PC V 5.03. Relevant information on the data collection and the figures of merit of final refinement are listed in Table 3.

Acknowledgment. The generous support from both the University of Miami (start-up fund and the funding for the CCD-diffractometer) and the Petroleum Research Fund/ACS(36595-AC3) is gratefully acknowledged. The author thanks Mr. G.-L. Xu for recording NMR and IR spectra and Professor A. Kaifer for insightful discussions about electrochemistry. Interest in dissymmetric alkynyl adducts was stimulated by the comment from an anonymous reviewer of our earlier manuscript (ref 8).

Supporting Information Available: Tables of all atomic positional and equivalent isotropic displacement parameters, anisotropic displacement parameters, all bond distances and bond angles, and torsion angles of compounds **2a** and **3b**, and tables of scan-rate dependence of voltammetric data of compounds **3a**/**b** and **4**. This material is available free of charge via the Internet at http://pubs.acs.org.

OM0109004

(22) *SHELXTL 5.03 (WINDOW−NT Version), Program library for Structure Solution and Molecular Graphics;* Bruker-AXS Inc., 1998.
(23) Sheldrick, G. M. *SHELXS-90, Program for the Solution of Crystal Structures*; University of Göttigen: Germany, 1990.
(24) Sheldrick, G. M. *SHELXL-93, Program for the Refinement of Crystal Structures*; University of Göttigen: Germany, 1993.